7-12-2012

Ionospheric Signatures of Tohoku-Oki Tsunami of March 11, 2011: Model Comparisons Near the Epicenter

David A. Galvan
RAND Corporation

Attila Komjathy
Jet Propulsion Laboratory, California Institute of Technology

Michael P. Hickey
Embry-Riddle Aeronautical University, hicke0b5@erau.edu

Philip Stephens
Jet Propulsion Laboratory, California Institute of Technology

Jonathan Snively
Embry-Riddle Aeronautical University, snivelyj@erau.edu

See next page for additional authors

Ionospheric signatures of Tohoku-Oki tsunami of March 11, 2011: Model comparisons near the epicenter

David A. Galvan,[1,2] Attila Komjathy,[1] Michael P. Hickey,[3] Philip Stephens,[1] Jonathan Snively,[3] Y. Tony Song,[1] Mark D. Butala,[1] and Anthony J. Mannucci[1]

Received 26 March 2012; revised 1 June 2012; accepted 6 June 2012; published 12 July 2012.

[1] We observe ionospheric perturbations caused by the Tohoku earthquake and tsunami of March 11, 2011. Perturbations near the epicenter were found in measurements of ionospheric total electron content (TEC) from 1198 GPS receivers in the Japanese GEONET network. For the first time for this event, we compare these observations with the estimated magnitude and speed of a tsunami-driven atmospheric gravity wave, using an atmosphere-ionosphere-coupling model and a tsunami model of sea-surface height, respectively. Traveling ionospheric disturbances (TIDs) were observed moving away from the epicenter at approximate speeds of 3400 m/s, 1000 m/s and 200–300 m/s, consistent with Rayleigh waves, acoustic waves, and gravity waves, respectively. We focus our analysis on gravity waves moving south and east of the epicenter, since tsunamis propagating in the deep ocean have been shown to produce gravity waves detectable in ionospheric TEC in the past. Observed southeastward gravity wave perturbations, seen ∼60 min after the earthquake, are mostly between 0.5 to 1.5 TECU, representing up to ∼5% of the background vertical TEC (VTEC). Comparisons of observed TID gravity waves with the modeled tsunami speed in the ocean and the predicted VTEC perturbation amplitudes from an atmosphere-ionosphere-coupling model show the measurements and models to be in close agreement. Due to the dense GPS network and high earthquake magnitude, these are the clearest observations to date of the effect of a major earthquake and tsunami on the ionosphere near the epicenter. Such observations from a future real-time GPS receiver network could be used to validate tsunami models, confirm the existence of a tsunami, or track its motion where in situ buoy data is not available.

Citation: Galvan, D. A., A. Komjathy, M. P. Hickey, P. Stephens, J. Snively, Y. Tony Song, M. D. Butala, and A. J. Mannucci (2012), Ionospheric signatures of Tohoku-Oki tsunami of March 11, 2011: Model comparisons near the epicenter, *Radio Sci.*, *47*, RS4003, doi:10.1029/2012RS005023.

1. Introduction

[2] A magnitude 9.0 earthquake occurred on March 11, 2011 at 05:46:23 Universal Time (UT) off the coast of Japan, heavily affecting the northern region of Tohoku, as well as the rest of the nation. The quake generated a major tsunami resulting in widespread casualties and destruction along the coast.

[3] Previous observations and modeling results have shown that earthquakes and tsunamis can produce acoustic and gravity waves that propagate up to the ionosphere, disturbing the electron density in the *F* region. Ionospheric disturbances caused by Rayleigh and acoustic waves due to earthquakes have been observed for many years [e.g., *Davies and Baker*, 1965; *Kelley et al.*, 1985; *Calais and Minster*, 1995], and have included recent observations of "co-seismic ionospheric disturbances" (CIDs) near Japan using the GEONET array [e.g., *Heki and Ping*, 2005; *Heki et al.*, 2006; *Astafyeva et al.*, 2009, *Rolland et al.*, 2011a]. Reports of ionospheric perturbations caused by the Tohoku-Oki seismic event itself have also been recently published [e.g., *Liu et al.*, 2011; *Rolland et al.*, 2011b; *Maruyama et al.*, 2011; *Matsumura et al.*, 2011; *Occhipinti et al.*, 2011; *Makela et al.*, 2011].

[4] For this study, we focus on the gravity waves observed in the ionosphere in the region near the epicenter of the Tohoku earthquake and tsunami. We investigate whether the tsunami contributed significantly to these atmospheric waves by comparing observations with modeling results.

[5] Modeling efforts have shown that atmospheric gravity waves caused by tsunamis should be detectable as traveling ionospheric disturbances (TIDs) [e.g., *Hines*, 1960, 1967, 1972; *Peltier and Hines*, 1976; *Occhipinti et al.*, 2006, 2008; *Hickey et al.*, 2009; *Mai and Kiang*, 2009]. Tsunami-driven

[1]Jet Propulsion Laboratory, California Institute of Technology, Pasadena, California, USA.
[2]Now at RAND Corporation, Santa Monica, California, USA.
[3]Embry Riddle Aeronautical University, Daytona Beach, Florida, USA.

Corresponding author: D. A. Galvan, RAND Corporation, 1776 Main St., Santa Monica, CA 90401, USA. (davidgalvan@gmail.com)

0048-6604/12/2012RS005023

TIDs have also been detected for previous events in ionospheric total electron content (TEC) using ground-based GPS radio signals [e.g., *Artru et al.*, 2005; *Rolland et al.*, 2010; *Galvan et al.*, 2011] and satellite altimeter radar [e.g., *Occhipinti et al.*, 2006].

[6] Prior to the Tohoku-Oki event, most ionospheric TEC perturbations caused by tsunamis have been observed far afield from the epicenter [e.g., *Artru et al.*, 2005; *Rolland et al.*, 2010; *Galvan et al.*, 2011]. While there have been previous investigations of ionospheric disturbances following major earthquakes using the dense Japanese GEONET array [e.g., *Heki and Ping*, 2005; *Astafyeva and Heki*, 2009; *Rolland et al.*, 2011a] those events were not accompanied by major tsunamis. Those studies therefore focused on the acoustic and Rayleigh waves produced by earthquakes alone, and did not observe strong gravity wave signatures in the ionosphere. For recent investigations involving tsunami-driven TIDs, only a few GPS receivers were typically available within several hundred to a thousand kilometers of the epicenters, providing poor coverage near the epicenter during the early stages of the tsunami [e.g., *Galvan et al.*, 2011]. Data sets originating from the region near the epicenter are critical to our understanding of the propagation of gravity waves from tsunamis. The Tohoku-Oki earthquake occurred very close to one of the most dense networks of GPS receivers in the world: Japan's GEONET network with an abundance of ionospheric TEC measurements in the vicinity of the epicenter available before, during, and after the tsunami moved through the region. Thus, this event presents a unique opportunity to image the ionospheric response to a major tsunami in its earliest stages. Since the earthquake had such a high magnitude, it is likely that both the earthquake and the tsunami contributed to disturbances observed in ionospheric total electron content. But one may ask: are the gravity wave perturbations caused largely by the tsunami or by the earthquake itself? We present comparisons with models of tsunami-sea-surface height and atmosphere-ionosphere-coupling, in order to assess whether the tsunami contributed significantly to the ionospheric disturbances observed near the epicenter.

2. Methodology

[7] Dual-frequency GPS receivers measure time delay and phase advance observables that can be processed to produce TEC data. There are several major networks of ground-based, dual-frequency GPS receivers that can be used for this purpose. We used data from Japan's GEONET network of over ~1200 GPS stations, publicly available for download from the Geospatial Information Authority (available at http://terras.gsi.go.jp/gps/geonet_top.html).

[8] We used the Global Ionospheric Mapping (GIM) [e.g., *Komjathy et al.*, 2005; *Mannucci et al.*, 1998] software suite to process the Receiver Independent Exchange format (RINEX) files from the GEONET network and infer calibrated TEC values between the ground GPS receivers and satellites at a time resolution of 30 s. Overall accuracy for absolute TEC values tends to be at the 1–2 TECU level [e.g., *Mannucci et al.*, 2004; *Komjathy et al.*, 2005], where 1 TECU = 10^{12} el/cm^2. Obtaining absolute TEC values is useful to understand background conditions for the perturbations. However, we are primarily interested in monitoring small-scale variations in ionospheric electron density, hence the changes in TEC are of interest, rather than absolute TEC values. The precision of TEC measurements using the GIM processing is typically of order 0.01 to 0.1 TECU [e.g., *Mannucci et al.*, 1998, 2004]. We use slant TEC measurements mapped to the vertical using a standard geometric mapping function [e.g., *Komjathy et al.*, 2005], thus producing estimates of vertical total electron content (VTEC).

[9] In order to remove longer period variations in TEC time series (such as diurnal variations and multiple-hour trends due to changing elevation angle of the receiver-satellite line-of-sight), we use a zero-phase bi-directional band-pass filter with a passband of 0.5 to 5 mHz (corresponding to wave periods of 2000 to 200 s; 33.3 min to 3.3 min) to extract variations in TEC with periods similar to that of the ocean tsunami itself (see *Galvan et al.* [2011] for detailed methodology).

[10] To image the TIDs, we compute ionospheric pierce points (IPPs): the geographic locations where the line-of-sight between GPS satellite and GPS receiver penetrates the ionospheric *F* region peak. The *F* region peak for this event was determined using JPL's Global Assimilative Ionosphere Model (GAIM) [e.g., *Komjathy et al.*, 2010], which ingested ground-based GPS and space-based radio-occultation TEC measurements from the COSMIC constellation in order to produce a profile of electron density as a function of altitude over the earthquake epicenter. The GAIM profiles over Japan revealed an *F* region peak at 300 km altitude. We used this as the altitude for locating our ionospheric pierce points and generating images of the TEC perturbations from the earthquake and tsunami.

[11] We compare the ionospheric TEC measurements to two different models: The Song model of sea surface height during the tsunami [e.g., *Song et al.*, 2012], and the Hickey model of atmosphere-ionosphere coupling [e.g., *Hickey et al.*, 2009]. The Song model uses high-precision position estimates from GPS receivers, along with known bathymetry, to infer seafloor motion. Subsequently, it estimates tsunami source energy and amplitude scales. We compare the geographic location and speed of the modeled tsunami wavefront with that of the ionospheric disturbances to the south and east of the epicenter. The Hickey model takes a given sea surface displacement, calculates the resulting amplitudes of atmospheric gravity waves and electron density perturbations in the ionosphere, and predicts the disturbance amplitude of VTEC, which we can compare directly to our observed GPS VTEC perturbations.

3. TEC Observations and Tsunami Model Comparisons

[12] We used 1198 available GEONET GPS stations to measure TEC perturbations within several thousand kilometers of the epicenter. (Some of the stations in Japan's network of over 1200 did not provide data suitable for this study due to power outages and loss-of-lock caused by the 9.0 magnitude quake.) In Figure 1 (left) the perturbations near the epicenter (defined by an arbitrary box 4 degrees by 4 degrees in latitude and longitude) are clearly seen as residual differences between measured slant TEC (STEC) and the GIM estimates for each measurement. The vertical line corresponds to the earthquake epoch at 5:46 UT (2:46

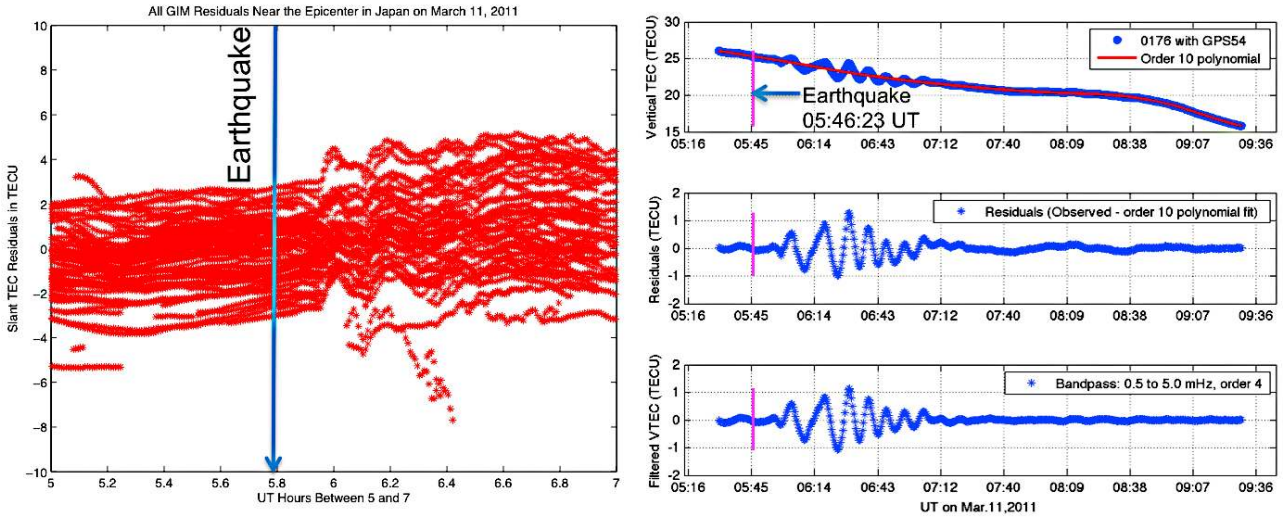

Figure 1. (left) GIM STEC residuals following the Tohoku-Oki earthquake. (right) An example of filtered VTEC observations for SVN 54 (PRN 18).

P.M. local) on March 11, 2011. In less than 10 min following the seismic event, the residuals indicate a signature consistent with the timing and magnitude of TEC perturbations initiated by an acoustic wave from the earthquake. One could imagine such a plot as the first available observations of an ionospheric disturbance immediately after a major quake has occurred, with only preliminary earthquake time and epicenter location from the USGS required to rapidly process and view the data.

[13] In Figure 1 (right), the upper plot displays the absolute vertical TEC (VTEC) values mapped from the STEC observed in the line-of-sight between GEONET Station 0176 and GPS satellite SVN 54 (PRN 18), along with a 10th order polynomial curve fit to the measurements. Polynomial fitting to the time series of TEC data is an alternative to bandpass filtering as a method for deriving TEC perturbations. The middle plot shows the residual differences between the polynomial fit and the actual observations. For this satellite track we see a signature with a period of ~10 min commencing about 10 min after the initial earthquake. The bottom plot indicates the variations in the absolute VTEC (top plot) after applying the band-pass filter. Applying this filtering process to the calibrated TEC data, using all GPS receivers available and all GPS satellites in view, is an effective means for resolving TEC variations that may be associated with the seismic activity and/or tsunami.

[14] The TEC perturbations on the middle and bottom plots are consistent with a propagation velocity of an acoustic wave generated by the earthquake [e.g., *Hickey et al.*, 2009; *Hines*, 1972]. An acoustic wave in the atmosphere caused by the earthquake would travel outward from the epicenter in all directions at the sound speed, which is approximately 1000 m/s at *F* region peak altitudes. In contrast, the tsunami travels with a horizontal speed of ~200–300 m/s away from the epicenter, creating an atmospheric gravity wave that propagates obliquely upward from the tsunami wavefront [e.g., *Galvan et al.*, 2011]. The vertical speed of the gravity wave (~50 m/s [e.g., *Artru et al.*, 2005; *Galvan et al.*, 2011]) is significantly lower than that of the acoustic wave. Therefore, the early perturbations shown in Figure 1 (right) emanating from the epicenter are most likely due to acoustic waves from the earthquake, though gravity waves are visible later, as discussed below. Examination of a single individual satellite-receiver pair time series is insufficient to establish with confidence whether a TEC perturbation is caused by a surface disturbance (such as an earthquake or tsunami) or some other source such as a geomagnetic disturbance. As such, it is important to analyze time series from many different receiver-satellite pairs in a geographic context.

[15] We generated geographic map images for the TEC perturbations using all 1198 available GEONET stations. Figure 2 is a series of map plots showing the progress of the TEC perturbations over time. Note that all time data in this paper are presented in UTC (UTC = GPS Time − 15 leap seconds, at the time of the Tohoku event). Each plot shows the band-pass filtered VTEC plotted in color (in units of TECU, with red-to-blue color bars on the right) at the location of the IPPs between the ground stations and up to 14 different GPS satellites. Each Japan-shaped group of IPPs represents one satellite in communication with all 1198 GEONET receivers. We show data from all available GPS satellites with elevation angles of 10 degrees and higher, with the exception of SVN 26 (PRN 26). (This satellite experienced significant data dropouts for receivers nearest the epicenter immediately after the earthquake, causing the bandpass filtering technique to produce distracting nonphysical artifacts.)

[16] Each plot also shows the sea-surface-height perturbation caused by the tsunami as predicted by the *Song et al.* [2012] model (in units of meters, with white-to-blue color bars on the left). This tsunami model takes into account seafloor motion measured by GPS receivers in the area during the earthquake, along with the bathymetry of the ocean floor, to produce a realistic simulation of tsunami waveform and speed. Figure 2a shows the IPPs just as the first acoustic and Rayleigh waves from the earthquake arrive at the *F* region peak of the ionosphere, causing the first VTEC disturbances. Figures 2b and 2c show the earthquake-generated acoustic and Rayleigh waves moving quickly away from the epicenter, as the white ocean tsunami wavefront makes

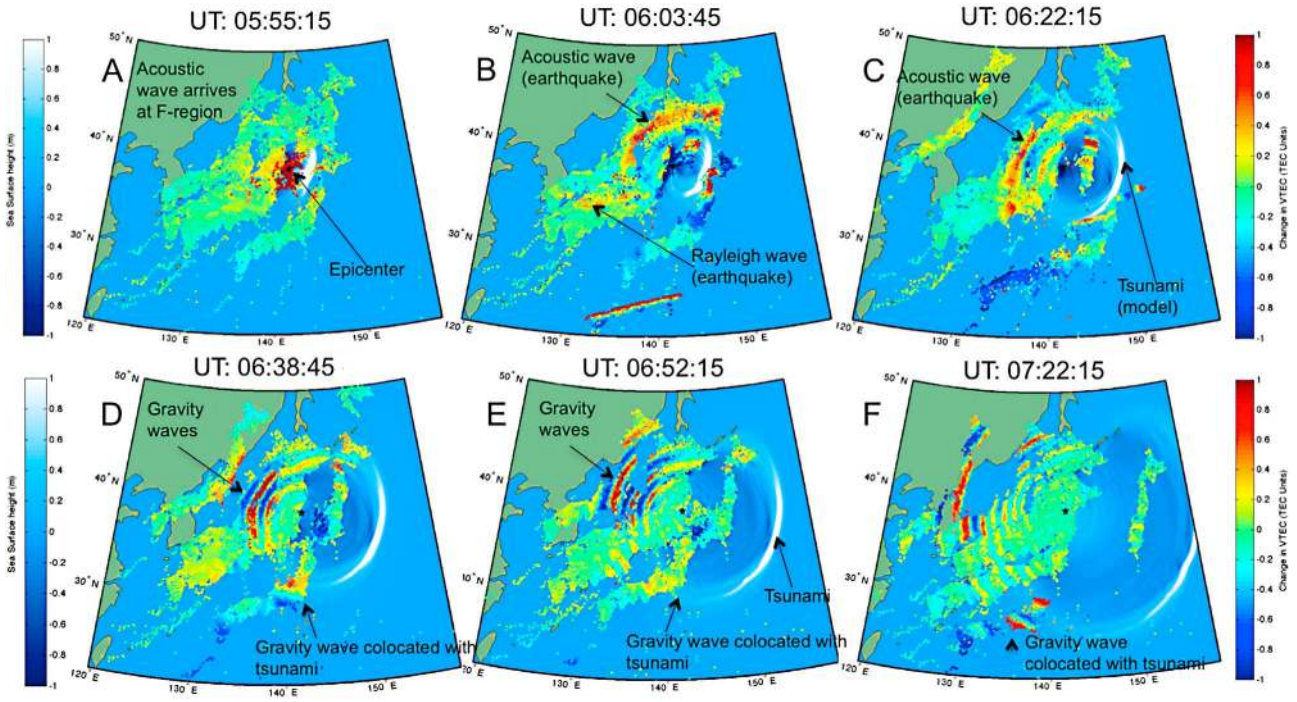

Figure 2. Map plots showing band-pass filtered VTEC (in units of TECU, right color bar) at ionospheric pierce points (IPPs) above Japan at different times on March 11, 2011. Each cluster of IPPs represents locations in the ionosphere where the signal from one GPS satellite, communicating with all GEONET receivers, passes through the *F* region peak at 300 km altitude. IPPs are plotted over sea surface heights from the Song tsunami model (in units of meters, left color bar) for comparison of wavefront positions in the ocean and ionosphere. These are frames from an animation available as dynamic content. (Animation S3)

progress as well. And Figures 2d through 2f show TIDs with gravity wave speeds moving away from the center at roughly the same speed as the ocean tsunami. In some regions (see plot annotations), the ionospheric gravity waves are roughly co-located with the ocean tsunami below.

[17] Animation S1 in the auxiliary material[1] depicts the waves in the ionospheric VTEC expanding out from the epicenter. Animation S2 shows only the Song model of sea surface wave heights for the Tohoku-Oki tsunami, without any ionospheric observations [e.g., *Song et al.*, 2012]. Animation S3 over-plots the ionospheric observations with the modeled sea-surface heights, as in Figure 2, showing the correlation of ionospheric TEC perturbations with the ocean wave below. Note this represents the first time that ionospheric TEC data has been directly compared to modeled sea surface heights in this manner for this event. Such comparisons may be useful during future tsunami scenarios, since TEC observations represent real measurements that can be compared with quickly generated tsunami models, such as the NOAA MOST model [e.g., *Titov and Gonzalez*, 1997] to verify tsunami location in near real time. This capability would be most useful in cases where the tsunami is moving through a region with few ocean buoys but potentially available GPS receivers.

[18] Animation S3 and Figures 2d–2f show that, while observations are sparse over the ocean far east of Japan, the modeled tsunami circular wavefront pattern in the south and east aligns with the gravity wave TIDs in the south and southwest, especially after 06:45 UT. Also, while the westward ocean tsunami is stymied by the islands of Japan (Animation S2), some TIDs move westward over and past the islands (Animations S1 and S3 and Figures 2d–2f). In addition, the gravity wave TIDs traveling toward the northwest over Japan have higher amplitudes in TEC than those moving in any other azimuthal direction.

[19] It is possible that these northwestward TIDs were partially driven by the earthquake through a direct excitation mechanism, where the original displacement of the ocean surface due to the earthquake generated a gravity wave independent of any propagating tsunami, as suggested by *Matsumura et al.*, 2011. It is also plausible that the westward portion of the tsunami generated westward atmospheric gravity waves before reaching the coast, and that those tsunami-driven gravity waves continued to propagate over Japan after the ocean wave was stopped at the coast, contributing to the observed TID. The westward traveling tsunami increased in amplitude as it approached the coast due to decreasing water depth, which could amplify the atmospheric gravity wave. This may be one reason why the observed TIDs are most intense in the northwestward direction as compared to other azimuthal directions: The combined gravity waves from the direct excitation mechanism and the westward propagating tsunami may have caused an enhanced TID in that direction.

[20] Such behavior, where ionospheric TIDs caused by tsunami-driven gravity waves have persisted beyond coastlines, has been previously observed [e.g., *Artru et al.*, 2005;

[1]Auxiliary materials are available in the HTML. doi:10.1029/2012RS005023.

Galvan et al., 2011]. This behavior is also consistent with theory, since the TEC measurements will only show signatures of the ocean surface waves after the internal gravity waves have had time to propagate obliquely from the surface up to the ionosphere. Hence, when a tsunami is stymied upon encountering a coastline, we would expect the associated TID to continue propagating horizontally for some distance beyond the coast, both as a result of the time for the termination of the gravity wave to reach the *F* region peak, and the time it would take for the TID to damp due to energy dissipation after it is no longer driven by the tsunami. Further modeling work (beyond the scope of this paper) is required to determine how significant a role the westward tsunami is playing in the northwestward TIDs observed moving over Japan. For the rest of this paper, we focus on the TIDs observed moving over the ocean toward the east, southwest, and northeast, since there are co-located TIDs and tsunami wavefronts in these regions.

[21] Another way to display TEC perturbations in the ionosphere is to use composite distance versus time plots (also known as "travel-time" plots in the seismic community) showing the TEC perturbations in color as a function of time and geographic distance to the earthquake epicenter. In such plots, perturbation troughs and crests traveling at a constant velocity are aligned with straight lines in distance versus time. The slopes of the lines indicate the horizontal speed of propagation in the ionosphere. By noting the slopes of the TEC perturbations in the travel-time plot, we can distinguish perturbations associated with Rayleigh surface-waves from the earthquake, which have typical horizontal speeds ~3400 m/s [e.g., *Artru et al.*, 2001; *Rolland et al.*, 2011a], acoustic waves from the earthquake with typical horizontal speeds of ~1000 m/s at the *F* region peak, and gravity waves, which have been observed in previous studies [e.g., *Artru et al.*, 2005; *Rolland et al.*, 2010; *Galvan et al.*, 2011] to have approximately the same horizontal speed in the ionosphere as the tsunami itself on the ocean surface (~200 – 300 m/s).

[22] Figure 3 shows several travel-time plots illustrating the observed ionospheric perturbations and modeled ocean tsunami within 1500 km of the earthquake epicenter, in all azimuthal directions. Figure 3a shows a travel-time plot for a single satellite (SVN 55, PRN 15) in communication with all 1198 receivers in Japan, with VTEC perturbations derived from the band-pass filter technique shown in color in units of TECU. A range of different wave speeds is visible, including acoustic waves (parallel to the 1000 m/s line), and gravity waves with a range of different speeds between 200 and 300 m/s. We include a gravity wave reference line with a slope of 240 m/s, an average wave speed for the Tohoku-Oki tsunami in this region, according to the Song model. (Note when viewing these plots that the reference lines will not necessarily lay directly on top of the perturbation. Rather, one should compare the slope of a perturbation to the slope of a reference line to infer the relative horizontal speed of that disturbance in the ionosphere.)

[23] While the single-satellite plot in Figure 3a is useful in demonstrating a spectrum of traveling ionospheric disturbances with different velocities, a composite plot of observations from multiple satellites can also demonstrate the coherence of these ionospheric wave structures as the waves move from the ionospheric pierce points of one satellite to the next. Also, in the potential application of monitoring tsunami-driven TIDs in real-time, it will not be immediately known which satellites will observe tsunami-driven signals and which will not. Hence, a composite plot with all available observations can be useful. Figure 3b shows such a composite plot for all available GPS satellites (excluding the problematic SVN/PRN 26). Since multiple satellite IPPs may overlap one another, the filtered VTEC has been plotted such that those perturbations with the highest amplitudes are plotted on the top layer of the figure, so as to remain visible. Also, to avoid excessive data processing artifacts due to low elevation angles and band pass filtering edge effects, we show only data for elevation angles higher than 30 degrees.

[24] In Figures 3a and 3b, there is a strong wave pattern aligned with slopes mostly parallel to the 240 m/s line. There are also slower gravity waves at later times, with lower slopes in the travel-time plot. It appears that the early gravity waves near the epicenter travel horizontally at slightly higher speed than the subsequent waves. This expected phenomenon was first discussed by *Hines* [1967] in the context of controlled nuclear explosions. We also note that gravity waves first appear near the epicenter approximately 30 min after the earthquake (near 6:14 UT in Figure 3b). Previous model estimates of the vertical propagation speed of internal gravity waves [e.g., *Hines*, 1960; *Artru et al.*, 2005; *Galvan et al.*, 2011] suggested it should take ~1.6 h or longer for a gravity wave generated at the surface to reach the *F* region peak. However, it may not be necessary for the gravity wave to reach the *F* region peak (300 km in this case) for perturbations to be visible in TEC. Such perturbations could potentially be visible when the waves reach the upper E and lower F regions.

[25] To further compare the ionospheric TIDs traveling at gravity wave speed, we consider the modeled and observed speeds of the tsunami. Tsunamis approximately follow the shallow water wave speed, $v = \sqrt{gh}$, where g is gravitational acceleration and h is the depth of the ocean. The center depth of the Japan Trench is approximately 7,400 m. This predicts an estimated wave speed of 269 m/s near the Japan Trench, and slower speeds in shallower water on either side (west and east) of the trench (~121 m/s to the northwest, where average depth 1.5 km, and 221 m/s to the east, where average depth ~5 km). Ocean buoys in NOAA's Deep-ocean Assessment and Reporting of Tsunamis (DART) network (http://www.ndbc.noaa.gov/dart.shtml), can provide measurements of the average tsunami speed between the epicenter and the buoy location, based on arrival time. For example, DART buoy # 21413, located 1,244 km southeast of the epicenter, observed the tsunami at 06:59 UT, 1 h and 13 min after the earthquake occurred, yielding an average speed measurement of ~284 m/s between the epicenter and the buoy. Different buoys measure slightly different average velocities (for instance DART 21419 measures an average speed of 243 m/s), since the tsunami speed varies with bathymetry, and hence azimuthal direction.

[26] Figure 3c shows a distance versus time plot for the sea surface heights of the Tohoku-Oki tsunami, based on the tsunami model of *Song et al.* [2012]. The Song model produces sea-surface height values in a 0.1 × 0.1 degree latitude/longitude grid, so the vertical axis in Figure 3c

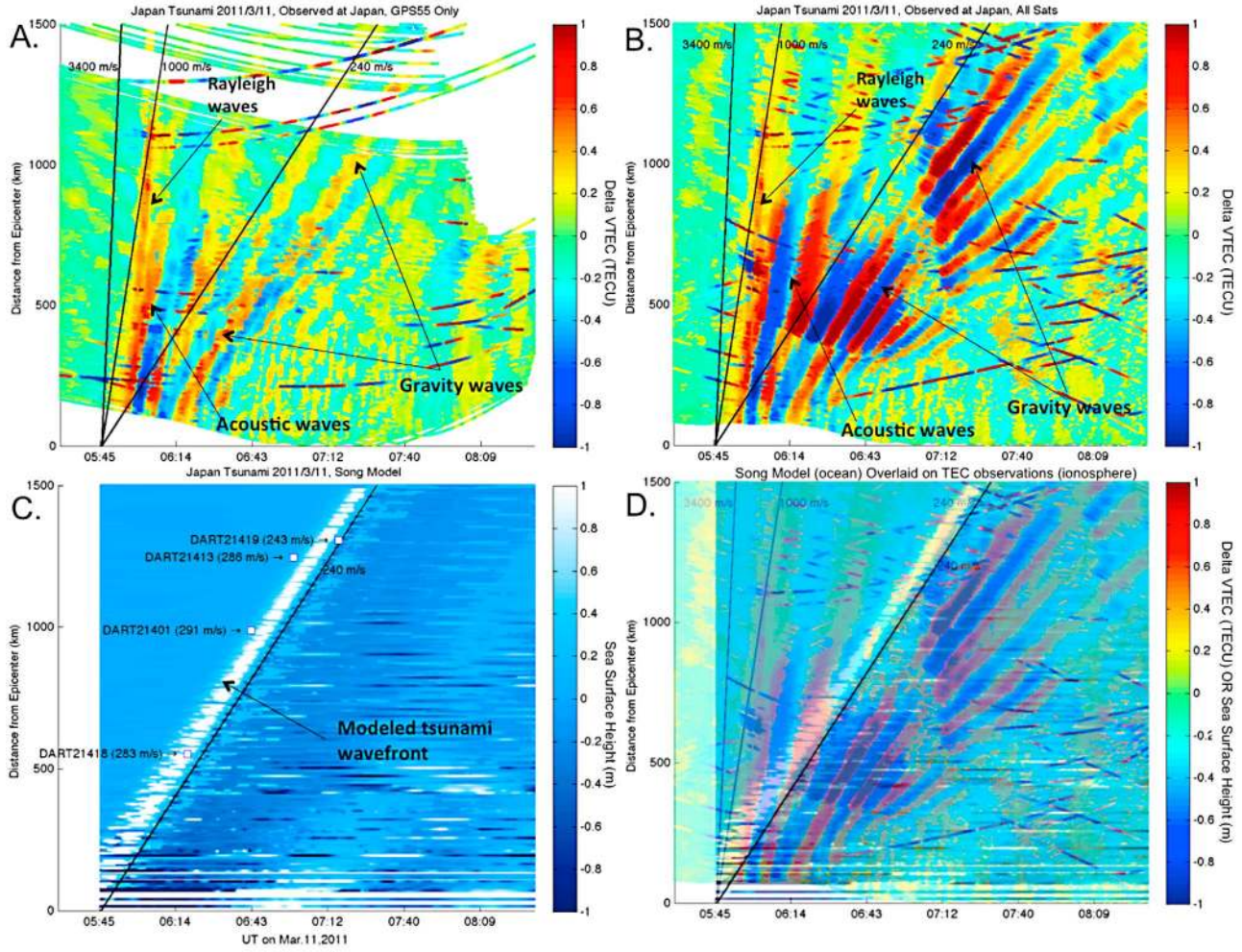

Figure 3. Travel-time plots for the region within 1500 km of the epicenter. Reference lines show the expected slope of waves traveling 3400 m/s (Rayleigh waves from the earthquake), 1000 m/s (acoustic waves from the earthquake), and 240 m/s (gravity waves from the tsunami). (a) Band-pass filtered VTEC perturbations for SVN 55 (PRN 15) only, shown in color, as a function of distance from the epicenter (vertical axis) and Universal Time (horizontal axis). (b) Band-pass filtered VTEC perturbations for all available GEONET stations (1198) and GPS satellites with elevation angles >30 deg. Highest amplitude variations are plotted on top layer to remain visible. (c) Song model [e.g., *Song et al.*, 2012] of sea surface height for the Tohoku tsunami. Color indicates sea surface height in meters. White squares show DART buoy position at time of tsunami arrival. (d) Figure 3c overlaid on Figure 4b.

represents the distance of each of those grid points from the earthquake epicenter. In this plot, the color represents the sea surface height in meters at each grid point and at each Universal Time. The 240 m/s reference line shown in Figures 3a and 3b was based on an azimuthally averaged fit to the Song model, as is evident by the reference line in 3c, parallel to the modeled tsunami wavefront. As "ground truth," the four DART buoys closest to the epicenter are also plotted at the buoy distance from the epicenter and the time at which each buoy first detected the tsunami, with average speeds annotated. Figure 3d displays the Song modeled sea-surface heights overlaid on the ionospheric TEC perturbations. Notice that the strongest gravity wave signals in the ionospheric observations are mostly parallel to (i.e., same speed as) the primary tsunami wavefront. Note this is the first time the position wavefronts of the ionospheric gravity wave and the modeled ocean tsunami have been directly compared with one another for this event.

[27] The TEC measurements in Figure 3 show ionospheric TIDs in all azimuthal directions around the epicenter. This means that, in addition to the eastward TIDs, the westward TIDs traveling over Japan are being compared with the tsunami model which is mostly traveling eastward (and southward and northeastward). We now focus on those observations moving away from Japan by simply separating out those IPPs that lie to the southeast of a geographical line going through the earthquake epicenter and approximately parallel to the eastern coast of Japan. Figure 4 shows a map plot similar to the plots in Figure 2, but only showing IPPs to the southwest of a rhumb line that goes through the earthquake epicenter at 38.32° latitude, 142.37° longitude (according to the USGS; see http://earthquake.usgs.gov/earthquakes/recenteqsww/Quakes/usc0001xgp.php), and remains

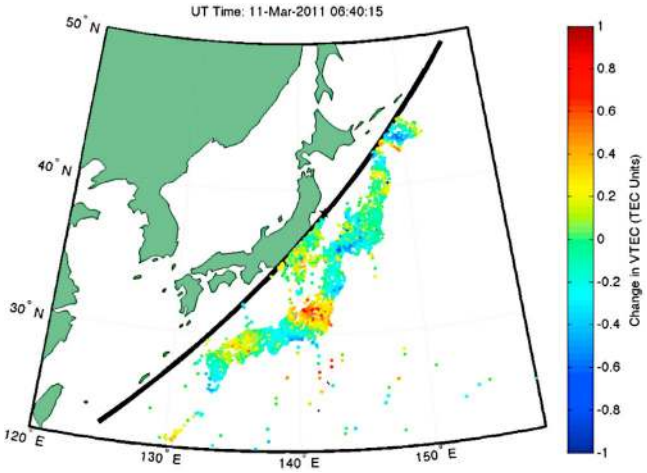

Figure 4. Map plot showing IPP locations to the southeast of a rhumb line in latitude and longitude that passes through the earthquake epicenter and continues approximately parallel to the Japanese islands. Only data points southeast of this line were included in Figure 5.

approximately parallel to the Japanese east coast. (A rhumb line crosses all meridians of longitude at the same angle. Here we use it as a simple method to separate those ionospheric pierce points which show approximately southeastward propagating TIDs from those which show northwestward propagating TIDs.) Figure 5 shows travel-time plots, similar to Figure 3, but excluding all IPPs to the northwest of the rhumb line shown in Figure 4. This excludes the strong northwestward TIDs moving over Japan, so we can focus only on the observed TIDs moving south, east, and northeast of the epicenter which can be directly compared with the modeled tsunami location. Figure 5a shows bandpass filtered VTEC from a single satellite (SVN 58), clearly showing gravity waves moving away from the epicenter. Figure 5b shows a travel-time plot that is comparable to Figure 3b, including all available satellites but, again, only showing measurements to the southeast of the curve shown in Figure 4. Note that, even without the strong westward TIDs, there are strong gravity wave signatures moving out over the ocean that are comparable to the tsunami wavefront, which is shown in Figure 5c. The gravity waves in Figure 5b, however, become apparent starting ~06:40 UT, approximately 54 min after the earthquake began and about 1000 km from the epicenter. This arrival time is reasonably consistent with the time it would take a tsunami-generated gravity wave to arrive at the *F* region, as discussed earlier. Acoustic waves from the earthquake are clearly visible in Figure 5b as well. Figure 5c shows the modeled tsunami overlaid on the ionospheric observations. Note that the main tsunami wavefront (white) overlays directly on the first gravity wave, which has a ~0.3 TECU amplitude (orange/yellow on the color scale).

4. Atmosphere-Ionosphere Coupling Model Comparison

[28] We have also used the atmosphere-ionosphere coupling model of *Hickey et al.* [2009] to estimate the expected perturbation to vertical TEC given the observed sea surface height displacement at a deep ocean buoy designed to monitor tsunami activity. This is the first time these TEC observations have been compared with a tsunami-driven atmosphere-ionosphere coupling model for this event. DART buoy # 21413, 1244 km southeast of the epicenter as mentioned earlier, observed average tsunami speed of ~284 m/s, with a sea surface height amplitude of 0.76 m and a period of 32 min (http://www.ndbc.noaa.gov/dart.shtml). Using this as input to the *Hickey et al.* [2009] model, we find an expected vertical TEC perturbation in the ionosphere of 5.3% of the background VTEC. Analysis of our observed TEC perturbations in the region near DART 21413 (Figure 5) reveals TEC perturbations as high 1.5 TECU, at a region and time where the background TEC was approximately 32 TECU. This yields a range of observed VTEC perturbations of up to (1.5 / 32 =) 4.7%, similar to the model-estimated VTEC perturbation 5.3%. Additional modeling efforts of this type are warranted to gain further insight.

[29] Any comparison between observations of tsunami-driven TID's from different events must be made with caution since the circumstances of every tsunami are different (propagation direction, earthquake magnitude, distance between measurement point and epicenter, wave period and amplitude at measurement point, etc.). However, we note that *Galvan et al.* [2011] used the model of *Hickey et al.* [2009] to calculate modeled VTEC perturbations from the Chile tsunami of February 2010 (as observed at Japan) to be 0.4% of the background, and from the Samoa tsunami of September 2009 (as observed at Hawaii) to be 1.4% of the background (compared with 5.3% for the Tohoku event, as mentioned above). The corresponding ranges of measured perturbations were 0.5% for the Chile event, 1.3% for the Samoa event, and 4.7% for the Tohoku event. The tsunami amplitudes at the modeled/measured points were 8 cm for the Chile event at Japan, 20 cm for the Samoa event at Hawaii, and 76 cm for the Tohoku event near the epicenter. More research is required to determine if these modeled data points from different events are representative of the general relationship between tsunami wave height and TEC perturbation magnitude.

5. Discussion

[30] The acoustic and Rayleigh waves generated by the earthquake typically require ~10 min to reach the ionosphere from the ocean surface, so they are soon detectable in the ionosphere. Indeed, as seen in Figures 3a and 3b, the earliest perturbations from the acoustic and Rayleigh waves for the Tohoku event are visible approximately 10 min after the earthquake. Gravity waves take longer due to much slower vertical group velocities. *Galvan et al.* [2011] used the vertical group velocity models of *Hines* [1960] and *Hickey and Cole* [1987] to estimate a lower limit arrival time of the tsunami-driven gravity wave at the *F* region peak of ~1.6 h. Prior to the Tohoku-Oki event, GPS receivers had not previously been so abundant near the epicenter of a major tsunamigenic earthquake to observe when the tsunami-driven gravity waves first arrive at the ionosphere. Hence, the tsunami signature was not expected to be observed near the epicenter, as after 1.6 h the tsunami-driven gravity waves would be approximately 1380 km from the epicenter before they could reach the *F* region peak (assuming a 240 m/s horizontal propagation speed to match the tsunami).

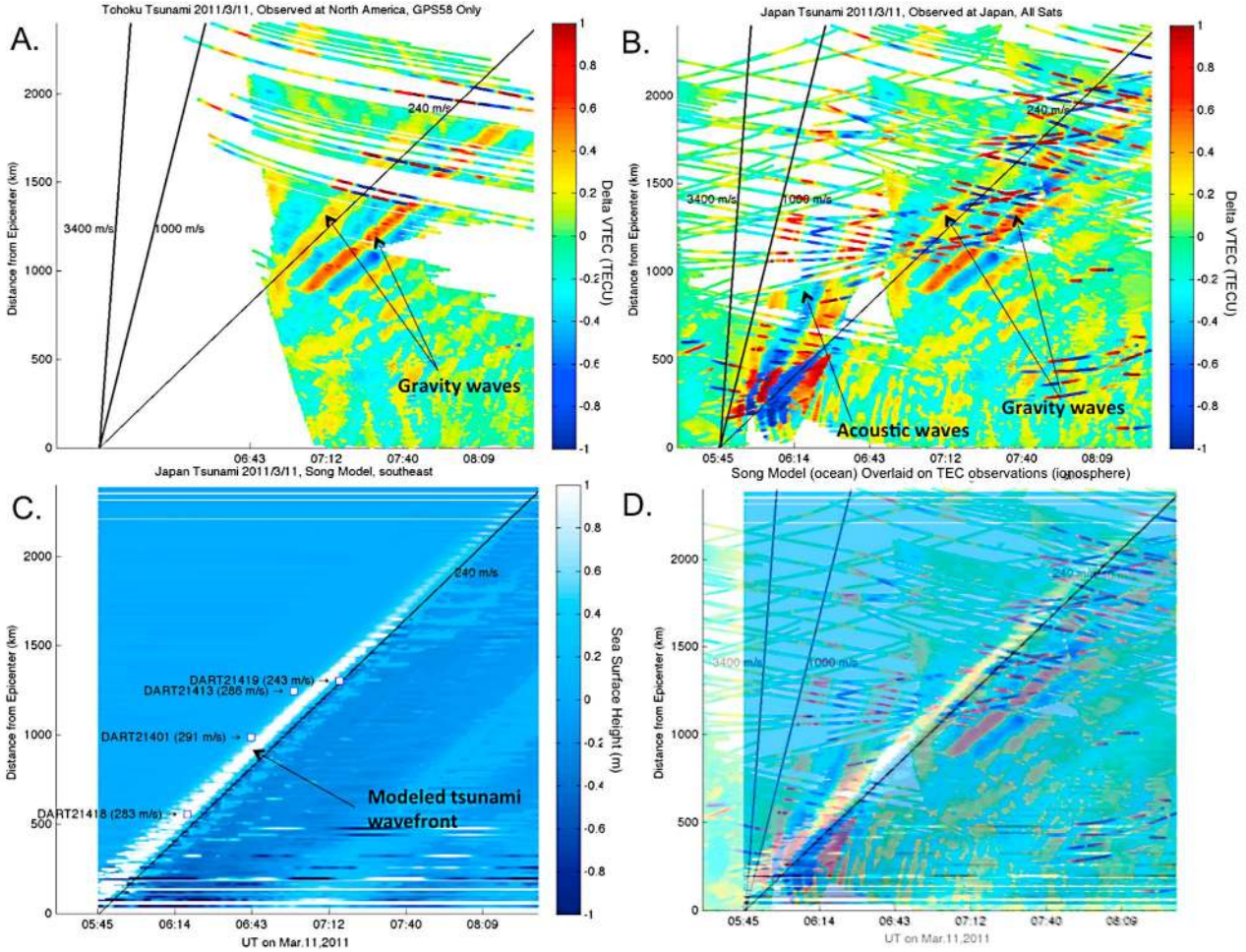

Figure 5. Travel-time plots for the region within 2400 km of the epicenter. Similar to Figure 3 but only showing observation points to the east, south, and southeast of a line through the epicenter parallel to the Japanese coast, to avoid comparing eastward modeled tsunami with westward observed TEC perturbations. (a) Band-pass filtered VTEC perturbations for SVN 58 only, shown in color, as a function of distance from the epicenter (vertical axis) and Universal Time (horizontal axis). (b) Band-pass filtered VTEC perturbations for all available GEONET stations (1198) and GPS satellites with elevation angles >30 deg. Highest amplitude variations are plotted on top layer to remain visible. (c) Song model [e.g., *Song et al.*, 2012] of sea surface height for the Tohoku tsunami. Color indicates sea surface height in meters. White squares show DART buoy position at time of tsunami arrival. (d) Figure 5c overlaid on Figure 5b.

[31] Figures 3a and 3b, however, show ~240 m/s waves, to the northwest of the epicenter, visible in the ionospheric TEC data as early as ~30 min after the earthquake. These waves remain coherent in propagation speed and direction for thousands of km. One possible explanation might be that this seismic event was of sufficient amplitude to perturb ionospheric electrons substantially below the *F* region peak at ~300 km altitude. We speculate that electrons in the *E* region (~120 km altitude) may be responsible for these early perturbations. Another possibility is higher-than-expected vertical propagation speeds. Additional analysis is required on this topic.

[32] If such TEC measurements were available in real time, a practical application would be the real-time monitoring of the position and intensity of the traveling ionospheric disturbance caused by the tsunami. In an ideal case, we could monitor the position of the tsunami signature in the ionosphere as it moves across the ocean. Of course, real time monitoring requires that we have an abundance of GPS receivers on coasts and islands in the relevant region. As the installation of dual frequency GPS receivers continues (e.g., for monitoring the motion of tectonic plates), we expect more opportunities to observe these traveling ionospheric disturbances in the future.

6. Conclusions

[33] We present observational evidence of the ionospheric signatures of a major earthquake and tsunami in the region

near the epicenter of the March 2011 Tohuku-Oki event. Observed VTEC perturbations (up to ~4.7% of background) are consistent with model predictions of 5.3% VTEC disturbance based on the atmosphere-ionosphere coupling model of *Hickey et al.*, 2009. Comparisons of the ionospheric observations with the Song model of tsunami sea-surface height amplitudes show that the gravity-wave-induced TIDs have similar velocity to the ocean tsunami below, and that the TIDs are often geographically co-located with the tsunami wavefront. We cannot rule out the possibility that the initial raising and lowering of the ocean surface caused by the earthquake itself generated significant gravity waves that may contribute to the TIDs we observe, especially those to the northwest of the epicenter, moving over Japan. However, when we focus on the tsunami propagation southeast of the epicenter, the atmosphere-ionosphere coupling model predicts that the tsunami should create a detectable disturbance in the ionosphere. The observed disturbance is in agreement with the speed of the tsunami, the location of the tsunami, and the expected VTEC perturbation amplitude. We conclude that the ocean tsunami made a significant contribution to the southeastward ionospheric disturbances observed in VTEC. The relative contribution of the tsunami-driven internal gravity waves, as compared to gravity waves generated by the earthquake itself, deserves further research. To the best of our knowledge, these are the first comparisons of GPS-derived TEC perturbations with tsunami modeling results for this event.

[34] The highly dense network of 1198 available GPS receivers in Japan, combined with the proximity and magnitude of the tsunami's seismic source has provided an unprecedented (though tragic) set of circumstances to observe the early after-effects of ocean-atmosphere-ionosphere coupling following a major submarine earthquake. For the first time, the Tohoku event allows us to observe the origin and evolution of traveling ionospheric disturbances caused by both a major earthquake and major tsunami near the epicenter.

[35] **Acknowledgments.** The authors would like to thank John LaBrecque of NASA Headquarters and the Earth Science and Interior NASA ROSES Grant (NNH07ZDA001N-ESI), which made this research possible. RINEX files from the Japanese GEONET network were provided by the Geospatial Information Authority (GSI), a part of the Japanese Ministry of Land, Infrastructure, Transport and Tourism. Data analysis and tsunami modeling work was performed at the Jet Propulsion Laboratory, California Institute of Technology under contract to the National Aeronautics and Space Administration. Atmosphere-Ionosphere coupling modeling work was performed at Embry Riddle Aeronautical University.

References

Artru, J., P. Lognonné, and E. Blanc (2001), Normal modes modelling of post-seismic ionospheric oscillations, *Geophys. Res. Lett.*, *28*, 697–700, doi:10.1029/2000GL000085.

Artru, J., V. Ducic, H. Kanamori, P. Lognonné, and M. Murakami (2005), Ionospheric detection of gravity waves induced by tsunamis, *Geophys. J. Int.*, *160*, 840–848, doi:10.1111/j.1365-246X.2005.02552.x.

Astafyeva, E., and K. Heki (2009), Dependence of waveform of near-field coseismic ionospheric disturbances on focal mechanisms, *Earth Planets Space*, *61*(2), 939–943.

Astafyeva, E., K. Heki, V. Kiryushkin, E. Afraimovich, and S. Shalimov (2009), Two-mode long-distance propagation of coseismic ionosphere disturbances, *J. Geophys. Res.*, *114*, A10307, doi:10.1029/2008JA013853.

Calais, E., and J. B. Minster (1995), GPS detection of ionospheric perturbations following the January 17, 1994, Northridge earthquake, *Geophys. Res. Lett.*, *22*, 1045–1048, doi:10.1029/95GL00168.

Davies, K., and D. M. Baker (1965), Ionospheric Effects Observed around the Time of the Alaskan earthquake of March 28, 1964, *J. Geophys. Res.*, *70*, 2251–2253, doi:10.1029/JZ070i009p02251.

Galvan, D. A., A. Komjathy, M. P. Hickey, and A. J. Mannucci (2011), The 2009 Samoa and 2010 Chile tsunamis as observed in the ionosphere using GPS total electron content, *J. Geophys. Res.*, *116*, A06318, doi:10.1029/2010JA016204.

Heki, K., and J. Ping (2005), Directivity and apparent velocity of the coseismic ionospheric disturbances observed with a dense GPS array, *Earth Planet. Sci. Lett.*, *236*, 845–855, doi:10.1016/j.epsl.2005.06.010.

Heki, K., Y. Otsuka, N. Choosakul, N. Hemmakorn, T. Komolmis, and T. Maruyama (2006), Detection of ruptures of Andaman fault segments in the 2004 great Sumatra earthquake with coseismic ionospheric disturbances, *J. Geophys. Res.*, *111*, B09313, doi:10.1029/2005JB004202.

Hickey, M. P., and K. D. Cole (1987), A quartic dispersion equation for internal gravity waves in the thermosphere, *J. Atmos. Terr. Phys.*, *49*, 889–899, doi:10.1016/0021-9169(87)90003-1.

Hickey, M. P., G. Schubert, and R. L. Walterscheid (2009), Propagation of tsunami-driven gravity waves into the thermosphere and ionosphere, *J. Geophys. Res.*, *114*, A08304, doi:10.1029/2009JA014105.

Hines, C. O. (1960), Internal atmospheric gravity waves at ionospheric heights, *Can. J. Phys.*, *38*, 1441–1481, doi:10.1139/p60-150.

Hines, C. O. (1967), On the nature of traveling ionospheric disturbances launched by low-altitude nuclear explosions, *J. Geophys. Res.*, *72*(7), 1877–1882, doi:10.1029/JZ072i007p01877.

Hines, C. O. (1972), Gravity waves in the atmosphere, *Nature*, *239*, 73–78, doi:10.1038/239073a0.

Kelley, M. C., R. Livingston, and M. McCready (1985), Large amplitude thermospheric oscillations induced by an earthquake, *Geophys. Res. Lett.*, *12*, 577–580, doi:10.1029/GL012i009p00577.

Komjathy, A., L. Sparks, B. D. Wilson, and A. J. Mannucci (2005), Automated daily processing of more than 1000 ground-based GPS receivers for studying intense ionospheric storms, *Radio Sci.*, *40*, RS6006, doi:10.1029/2005RS003279.

Komjathy, A., B. Wilson, X. Pi, V. Akopian, M. Dumett, B. Iijima, O. Verkhoglyadova, and A. J. Mannucci (2010), JPL/USC GAIM: On the impact of using COSMIC and ground-based GPS measurements to estimate ionospheric parameters, *J. Geophys. Res.*, *115*, A02307, doi:10.1029/2009JA014420.

Liu, J.-Y., C.-H. Chen, C.-H. Lin, H.-F. Tsai, C.-H. Chen, and M. Kamogawa (2011), Ionospheric disturbances triggered by the 11 March 2011 *M*9.0 Tohoku earthquake, *J. Geophys. Res.*, *116*, A06319, doi:10.1029/2011JA016761.

Mai, C.-L., and J.-F. Kiang (2009), Modeling of ionospheric perturbation by 2004 Sumatra tsunami, *Radio Sci.*, *44*, RS3011, doi:10.1029/2008RS004060.

Makela, J. J., et al. (2011), Imaging and modeling the ionospheric airglow response over Hawaii to the tsunami generated by the Tohoku earthquake of 11 March 2011, *Geophys. Res. Lett.*, *38*, L00G02, doi:10.1029/2011GL047860.

Mannucci, A. J., B. D. Wilson, D. N. Yuan, C. H. Ho, U. J. Lindqwister, and T. F. Runge (1998), A global mapping technique for GPS-derived ionospheric total electron content measurements, *Radio Sci.*, *33*, 565–582, doi:10.1029/97RS02707.

Mannucci, A. J., et al. (2004), GPS-based remote sensing of the geospace environment: Horizontal and vertical structure of the ionosphere and plasmasphere, *Proc. SPIE Int. Soc. Opt. Eng.*, *5660*, 1–13, doi:10.1117/12.580048.

Maruyama, T., T. Tsugawa, H. Kato, A. Saito, Y. Otsuka, and M. Nishioka (2011), Ionospheric multiple stratifications and irregularities induced by the 2011 Tohoku earthquake, *Earth Planets Space*, *63*(7), 869–873, doi:10.5047/eps.2011.06.008.

Matsumura, M., A. Saito, T. Iyemori, H. Shinagawa, T. Tsugawa, Y. Otsuka, M. Nishioka, and C. H. Chen (2011), Numerical simulations of atmospheric waves excited by the 2011 off the Pacific coast of Tohoku Earthquake, *Earth Planets Space*, *63*(7), 885–889, doi:10.5047/eps.2011.07.015.

Occhipinti, G., P. Lognonné, E. A. Kherani, and H. Hébert (2006), Three-dimensional waveform modeling of ionospheric signature induced by the 2004 Sumatra tsunami, *Geophys. Res. Lett.*, *33*, L20104, doi:10.1029/2006GL026865.

Occhipinti, G., E. A. Kherani, and P. Lognonné (2008), Geomagnetic dependence of ionospheric disturbances induced by tsunamigenic internal gravity waves, *Geophys. J. Int.*, *173*, 753–765, doi:10.1111/j.1365-246X.2008.03760.x.

Occhipinti, G., P. Coïsson, J. J. Makela, S. Allgeyer, A. Kherani, H. Hébert, and P. Lognonné (2011), Three-dimensional numerical modeling of tsunami-related internal gravity waves in the Hawaiian atmosphere, *Earth Planets Space*, *63*(7), 847–851, doi:10.5047/eps.2011.06.051.

Peltier, W. R., and C. O. Hines (1976), On the possible detection of tsunamis by a monitoring of the ionosphere, *J. Geophys. Res.*, *81*(12), 1995–2000.

Rolland, L. M., G. Occhipinti, P. Lognonné, and A. Loevenbruck (2010), Ionospheric gravity waves detected offshore Hawaii after tsunamis, *Geophys. Res. Lett.*, *37*, L17101, doi:10.1029/2010GL044479.

Rolland, L. M., P. Lognonné, and H. Munekane (2011a), Detection and modeling of Rayleigh wave induced patterns in the ionosphere, *J. Geophys. Res.*, *116*, A05320, doi:10.1029/2010JA016060.

Rolland, L. M., P. Lognonné, E. Astafyeva, E. Alam Kherani, N. Kobayashi, M. Mann, and H. Munekane (2011b), The resonant response of the ionosphere imaged after the 2011 off the Pacific coast of Tohoku Earthquake, *Earth Planets Space*, *63*(7), 853–857, doi:10.5047/eps.2011.06.020.

Song, Y. T., I. Fukumori, C. K. Shum, and Y. Yi (2012), Merging tsunamis of the 2011 Tohoku-Oki earthquake detected over the open ocean, *Geophys. Res. Lett.*, *39*, L05606, doi:10.1029/2011GL050767.

Titov, V. V., and F. Gonzalez (1997), Implementing and testing of the Method of Splitting Tsunami (MOST) model, *NOAA Tech. Memo. ERL PMEL-112*, Pac. Mar. Environ. Lab, Seattle, Wash.